NANO · MICRO small
www.small-journal.com

A Photosensitive Polymeric Carrier with a Renewable Singlet Oxygen Reservoir Regulated by Two NIR Beams for Enhanced Antitumor Phototherapy

*Chun Yang, Meihui Su, Pei Luo, Yanan Liu, Feng Yang, and Changhua Li**

Photodynamic therapy (PDT), which utilizes photosensitizer to convert molecular oxygen into singlet oxygen ($^1O_2$) upon laser irradiation to ablate tumors, will exacerbate the already oxygen shortage of most solid tumors and is thus self-limiting. Herein, a sophisticated photosensitive polymeric material (An-NP) that allows sustained $^1O_2$ generation and sufficient oxygen supply during the entire phototherapy is engineered by alternatively applying PDT and photothermal therapy (PTT) controlled by two NIR laser beams. In addition to a photosensitizer that generates $^1O_2$, An-NP consists of two other key components: a molecularly designed anthracene derivative capable of trapping/releasing $^1O_2$ with superior reversibility and a dye J-aggregate with superb photothermal performance. Thus, in 655 nm laser-triggered PDT process, An-NP generates abundant $^1O_2$ with extra $^1O_2$ being trapped via the conversion into EPO-NP; while in the subsequent 785 nm laser-driven PTT process, the converted EPO-NP undergoes thermolysis to liberate the captured $^1O_2$ and regenerates An-NP. The intratumoral oxygen level can be replenished during the PTT cycle for the next round of PDT to generate $^1O_2$. The working principle and phototherapy efficacy are preliminarily demonstrated in living cells and tumor-bearing mice, respectively.

1. Introduction

Photodynamic therapy (PDT), a clinically approved antitumor modality, has attracted increasing attention due to its distinct advantages including minimal invasiveness, high therapeutic accuracy, low systemic toxicity, to name a few.[1–3] In a typical PDT process, under light irradiation, the photosensitizer (PS) transfers the photoexcited energy of the triplet excited state to nearby oxygen molecules to generate singlet oxygen ($^1O_2$), which leads to efficient ablation of malignant cells and tissues.[4–8] Remarkably, PDT can provoke an immune response,[2,9] which renders it truly promising. However, aggressive cellular proliferation and insufficient neovascularization in fast-growing solid tumors result in severe O_2 deficiency,[10–18] which substantially decreases the treatment outcome of oxygen-dependent PDT.[19–22] Moreover, the oxygen consumption during PDT will further aggravate the tumor hypoxia, probably leading to cancer metastasis.[13,23]

Recently, fractional PDT (*f*PDT) with intermittent light irradiation has been developed to allow oxygen replenishment between two PDT cycles.[24–27] Compared with traditional PDT, *f*PDT is promising to relieve photo-induced tumor hypoxia during light treatment. To further enhanced the *f*PDT efficacy, Akkaya et al.[28] introduced a 2-pyridone module in the PS design as a renewable $^1O_2$ reservoir to capture $^1O_2$ in the light cycle and release it in the dark cycle, thereby enabling sustained $^1O_2$ generation during *f*PDT. However, the $^1O_2$-trapped product of 2-pyridone, that is, endoperoxide (EPO), underwent a spontaneous cycloreversion reaction to release $^1O_2$ in an uncontrolled manner. In contrast, remote control of the smooth release of $^1O_2$ from the generated EPO during the oxygen replenishment process is expected to realize the full potential of *f*PDT.[29] EPOs of anthracene were demonstrated to produce $^1O_2$ upon heating[29–37] and thus have been applied as $^1O_2$ carriers to achieve remote light-controlled $^1O_2$ release by incorporation with photothermal agents (PTAs).[38,39] However, due to the lack of a suitable anthracene molecule that is capable of proceeding both a highly efficient cycloaddition reaction to trap $^1O_2$ to generate EPO and an efficient and clean thermo-induced cycloreversion reaction of EPO to liberate $^1O_2$, anthracene has not been used as a renewable $^1O_2$ reservoir for *f*PDT.

Herein, through rational molecular design, we successfully obtained a novel anthracene molecule (An-3) that presents reversible and clean switching between An and EPO states accompanied by $^1O_2$ trapping and releasing. In addition to the thermo-induced renewable $^1O_2$ reservoir with high quality, we also introduced a pure organic PTA based on BODIPY J-aggregate (^{J}BDP), which displays significant photothermal performance including red-shifted absorbance into the NIR region (785 nm), high photothermal conversion capability (PCE = 59.8%), and significant photobleaching resistance, to realize remote light-controlled $^1O_2$ release based on photothermy. By co-assembling with an amphiphilic diblock

C. Yang, Dr. M. Su, P. Luo, Y. Liu, F. Yang, Prof. C. Li
State Key Laboratory of Medicinal Chemical Biology
College of Pharmacy
Key Laboratory of Functional Polymer Materials of Ministry of Education
Nankai University
Tianjin 300071, P. R. China
E-mail: chli@nankai.edu.cn

The ORCID identification number(s) for the author(s) of this article can be found under https://doi.org/10.1002/smll.202101180.

DOI: 10.1002/smll.202101180

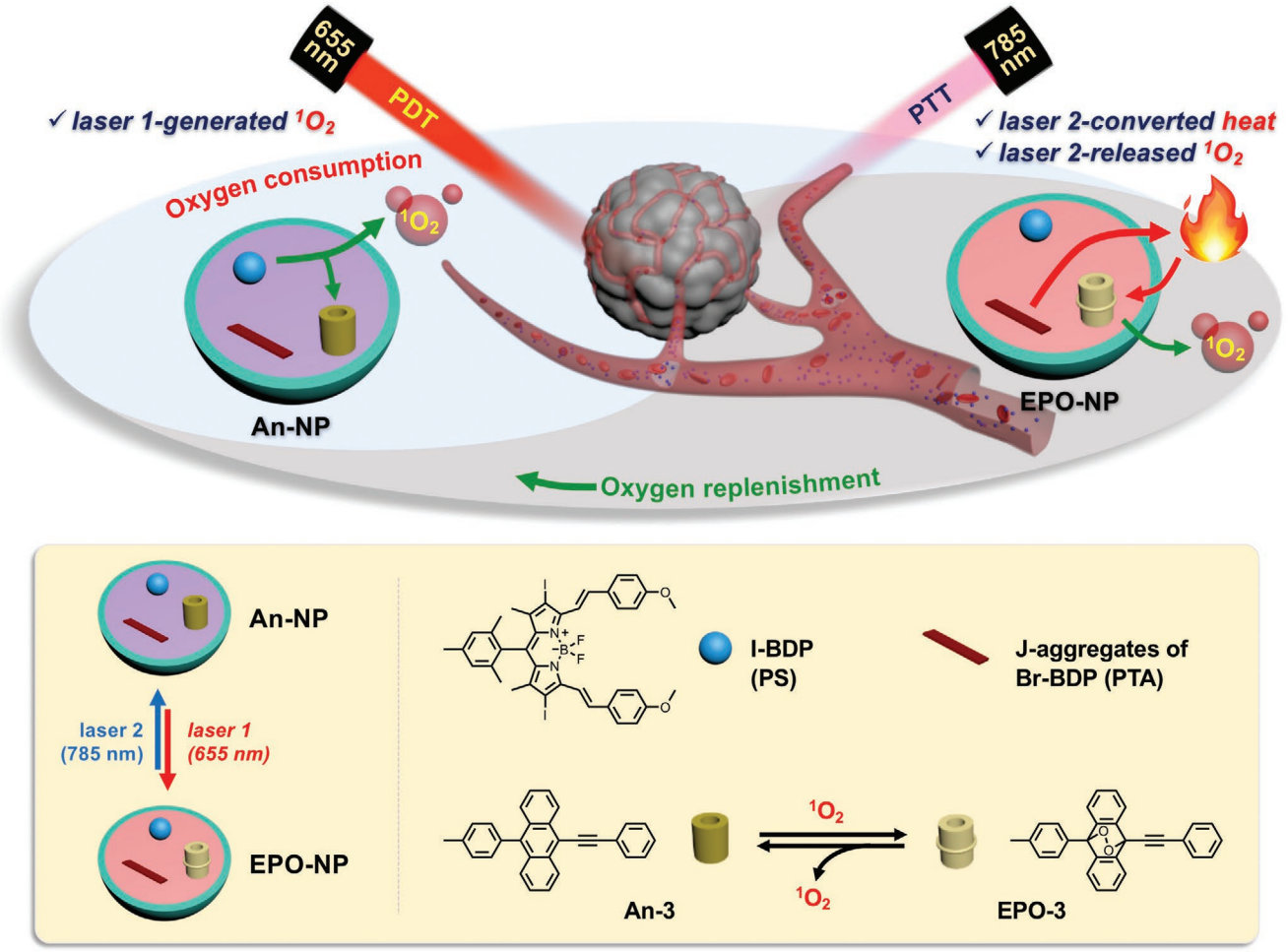

Scheme 1. Schematic illustration of the photosensitive polymeric nanoparticle (An-NP) with a renewable singlet oxygen ($^1O_2$) reservoir controlled by two laser beams for enhanced fractional PDT (*f*PDT). PS and PTA represent photosensitizer and photothermal agent, respectively.

copolymer, three key components, that is, a $^1O_2$ reservoir (An-3), a PTA (^{I}BDP), and a PS (I-BDP), were orchestrated in a single nanosystem to construct a sophisticated photosensitive nanomaterial (An-NP) for antitumor *f*PDT (**Scheme 1**). As detailed below, upon NIR laser-1 irradiation (655 nm), An-NP generates abundant $^1O_2$ with excessive $^1O_2$ being stored by forming EPO-NP; while after NIR laser-2 irradiation (785 nm), the converted EPO-NP undergoes thermolysis to release the trapped $^1O_2$ and regenerates An-NP. The oxygen level in the tumor should be replenished in the PTT process for the next round of PDT to generate $^1O_2$. For the first time, there is a single nanosystem that enables sustained $^1O_2$ generation and sufficient oxygen supply during the *f*PDT process by alternatively applying PDT and PTT regulated by two NIR laser beams. Dual-light irradiation can provide more controllability and has recently been widely used in multiple biological and biomedical fields, such as cancer treatment,[21] antibacterial,[40] photopharmacology,[41] optogenetics,[42] and optical-control of protein function and signaling,[43–45] etc. Moreover, the replacement of the dark cycle of conventional *f*PDT with PTT further enhanced the overall outcome of the anticancer phototherapy due to the synergistic effect of PDT and PTT (**Scheme 2**).[46–50]

2. Results and Discussion

2.1. Molecular Design of Anthracene Derivatives for $^1O_2$ Reservation

A renewable chemical reservoir of $^1O_2$ is the key to achieving sustained release of $^1O_2$ in the *f*PDT process. An ideal $^1O_2$ reservoir should store $^1O_2$ generated in PDT cycle and release it in a controlled manner during the interval between two PDT cycles. Anthracene (An) derivatives have been recognized as reliable $^1O_2$ carriers as they react with $^1O_2$ to form EPOs which can undergo cycloreversion reactions when heated to release the stored $^1O_2$ (**Figure 1**a). It has been reported that the substituents in the 9,10-positions of anthracene could substantially affect both cycloaddition and cycloreversion reactions in organic solvents.[37] However, the substituent-effect of anthracene in aqueous media has yet been studied. Aiming at obtaining a reliable anthracene-based $^1O_2$ reservoir that has to work in aqueous environment of living system, a set of anthracene derivatives (An-1, An-2, and An-3) with different 9,10-substituents were designed and successfully synthesized as outlined in **Scheme 3**. Then, an amphiphilic diblock copolymer,

	cycle 1		cycles ...
➢ Conventional	*laser* ➢ PDT	*dark* ➢ O_2 replenishment	*laser/dark*
✓ This work	*laser-1* ➢ PDT ✓ $^1O_2$ storing	*laser-2* ➢ O_2 replenishment ✓ Release of the stored $^1O_2$ ✓ Additional PTT for synergetic phototherapy	*laser-1/2*

Scheme 2. Conventional fractional PDT (*f*PDT) with intermittent light irradiation allowing oxygen replenishment between two PDT cycles; the designed enhanced-*f*PDT with sustained $^1O_2$ generation and additional PTT between two PDT cycles.

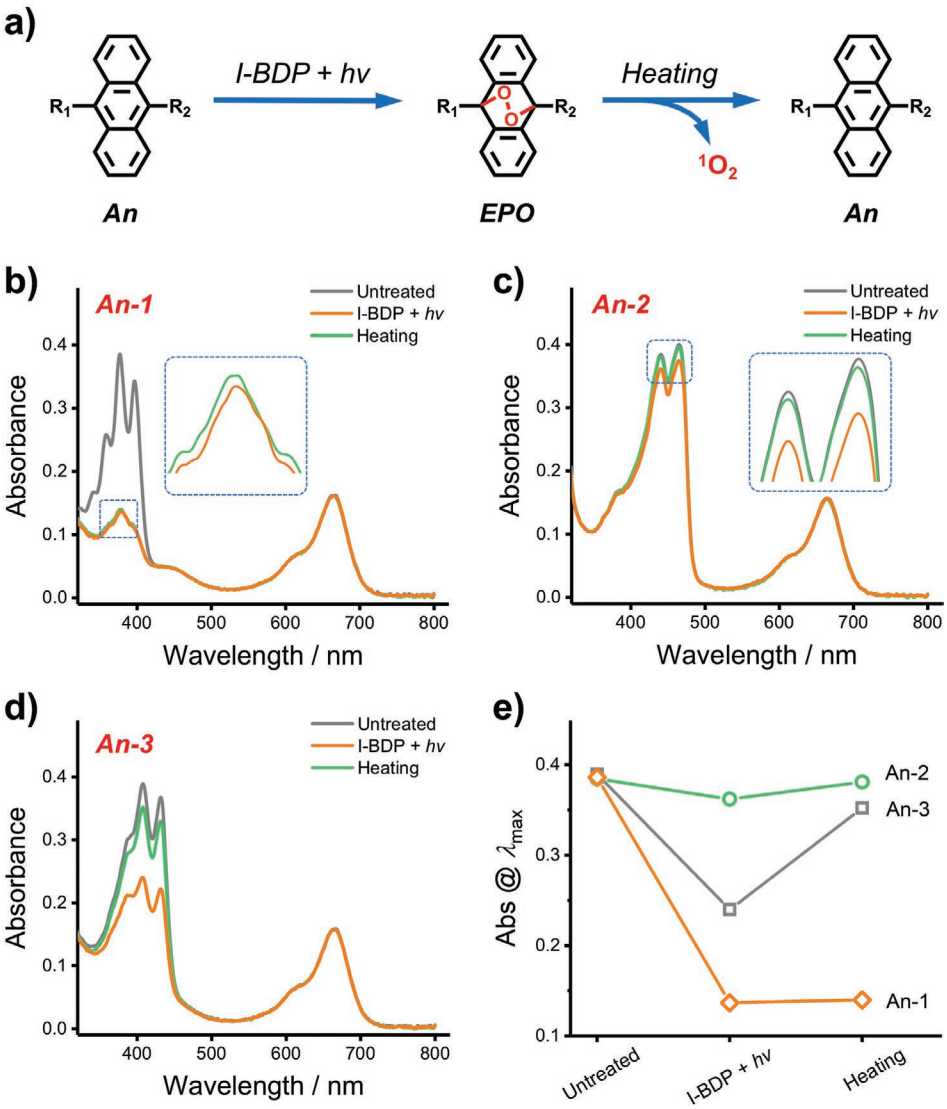

Figure 1. a) Cycloaddition reaction between anthracene (An) with the photogenerated singlet oxygen ($^1O_2$) yields EPO, which undergoes thermo-induced cycloreversion to restore An and release $^1O_2$. b–d) UV–vis absorption spectra and e) the absorbance at absorption maximum (Abs @ λmax) recorded for An-1 (b), An-2 (c), and An-3 (d) before and after sequential $^1O_2$ and thermal treatments; insets of (b) and (c) show an enlarged view of the area marked with a blue rectangle. $^1O_2$ was generated by I-BDP (2.3 μM) upon laser-1 irradiation. Laser-1: 655 nm, 10 mW cm^{-2}.

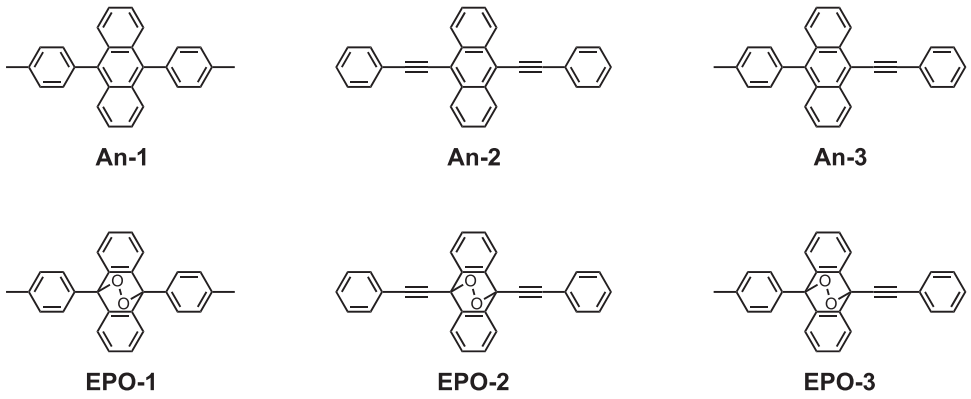

Scheme 3. Chemical structures of three anthracene (An) derivatives and the corresponding EPO.

poly(ethylene glycol)-block-poly(ε–caprolactone) (denoted as PEG-PCL) was employed to stabilize the hydrophobic anthracene derivatives via forming water-stable micelles. In the hydrophobic cores of the three formed micelles (An-1 micelle, An-2 micelle, and An-3 micelle), a PS (I-BDP) and different anthracene derivatives were embedded. The hydrodynamic sizes (Figure S1, Supporting Information) and the An-loading contents (Figure 1b–d) of the three micelles have been investigated by dynamic light scattering (DLS) test and UV–vis spectroscopy, respectively.

We further evaluated the $^1O_2$ trapping and releasing capability of the three anthracene derivatives, that is, An-1, An-2, and An-3, in aqueous media using UV–vis absorption spectroscopy. Upon laser-1 irradiation (655 nm; 10 mW cm^{-2}), the embedded I-BDP will generate $^1O_2$, and then reacts with anthracene to form EPO, resulting in the decrease in the absorption band of anthracene. Upon heating, the formed EPO can undergo cycloreversion to release the trapped $^1O_2$ and convert back to anthracene, leading to an increase in the absorption band. As shown in Figure 1b, with two phenyl moieties at 9,10 positions, An-1 displayed active cycloaddition reaction with $^1O_2$, while the formed EPO (EPO-1) showed negligible cycloreversion activity of releasing $^1O_2$ (Figure 1b,e). In stark contrast, An-2 substituted with two phenylethynyl groups showed much weaker cycloaddition activity with $^1O_2$, but the EPO-2 product had almost quantitative cycloreversion reactivity (Figure 1c). Notably, the consumed and restored amounts of anthracene derivatives during irradiation and heat process, respectively, were calculated and summarized in **Table 1**.

The above results clearly indicated that phenyl substituent effectively promotes the cycloaddition process of anthracene to capture $^1O_2$, while phenylethynyl substituent is beneficial to achieving the clean cycloreversion of EPO to release the trapped $^1O_2$. As expected, the respective introduction of a phenyl and a phenylethynyl substituent at the 9,10 positions of anthracene scaffold endowed the derivative, An-3, with both favorable cycloaddition and cycloreversion activities (Figure 1d,e). Moreover, compared with its organic solution, An-3 loaded in polymeric micelle displayed stronger $^1O_2$ trapping capability (Figure S5, Supporting Information). This should be attributed to the closer proximity between An-3 and I-BDP in the micelle core, which allows more $^1O_2$ to be trapped by An-3. The thermo-controlled cycloreversion of its EPO (EPO-3) was further studied. As shown in Figure S6, Supporting Information, inappreciable change in the absorption spectra of the aqueous EPO-3 solution at room temperature was observed over 24 h, indicating the stability of EPO-3 in water. Upon gradually elevating the temperature (37–90 °C), absorbance of the thermo-converted An-3 at 408 nm increased more abruptly (Figure S7, Supporting Information). Given the striking $^1O_2$-capturing and thermo-controlled O_2-releasing performance, An-3 was selected as the $^1O_2$ reservoir to construct the final nanosystem.

2.2. Stable J-Aggregation of BODIPY as the PTA

PTA can absorb light energy and convert it into heat, thereby inducing the thermolysis of EPO to release singlet oxygen. We then decided to utilize the concept of light-to-heat conversion of PTAs to realize the photo-controlled release of singlet oxygen. In contrast to inorganic PTAs which possess potential long-term in vivo toxicity,[51,52] biocompatible organic PTAs are more suitable for in vivo applications. However, several weaknesses of most organic PTAs, such as low PCE and weak resistance against photobleaching, substantially hampered their applications in

Table 1. The optical properties and $^1O_2$ trapping/releasing capabilities of anthracene derivatives.

Compound[a)]	λ_{Abs}[a)]/nm	ε[a)]/cm^{-1} M^{-1}	An-to-EPO[b)]/μmol	EPO-to-An[c)]/μmol
An-1	376	15 500	16.1	0.2
An-2	465	44 700	0.5	0.4
An-3	408	23 900	6.3	4.7

[a)]The compound was embedded in PEG-PCL micelle and data were collected in water; [b)]The compound and I-BDP were embedded in PEG-PCL micelle which was exposed to laser-1 irradiation for 2 min. An-to-EPO represents the amount of the produced EPO estimated by UV–vis spectroscopy. Laser-1: 655 nm, 10 mW cm^{-2}; [c)]The sample was subjected to heating at 80 °C for 30 min. EPO-to-An represents the amount of the restored An estimated by UV–vis spectroscopy.

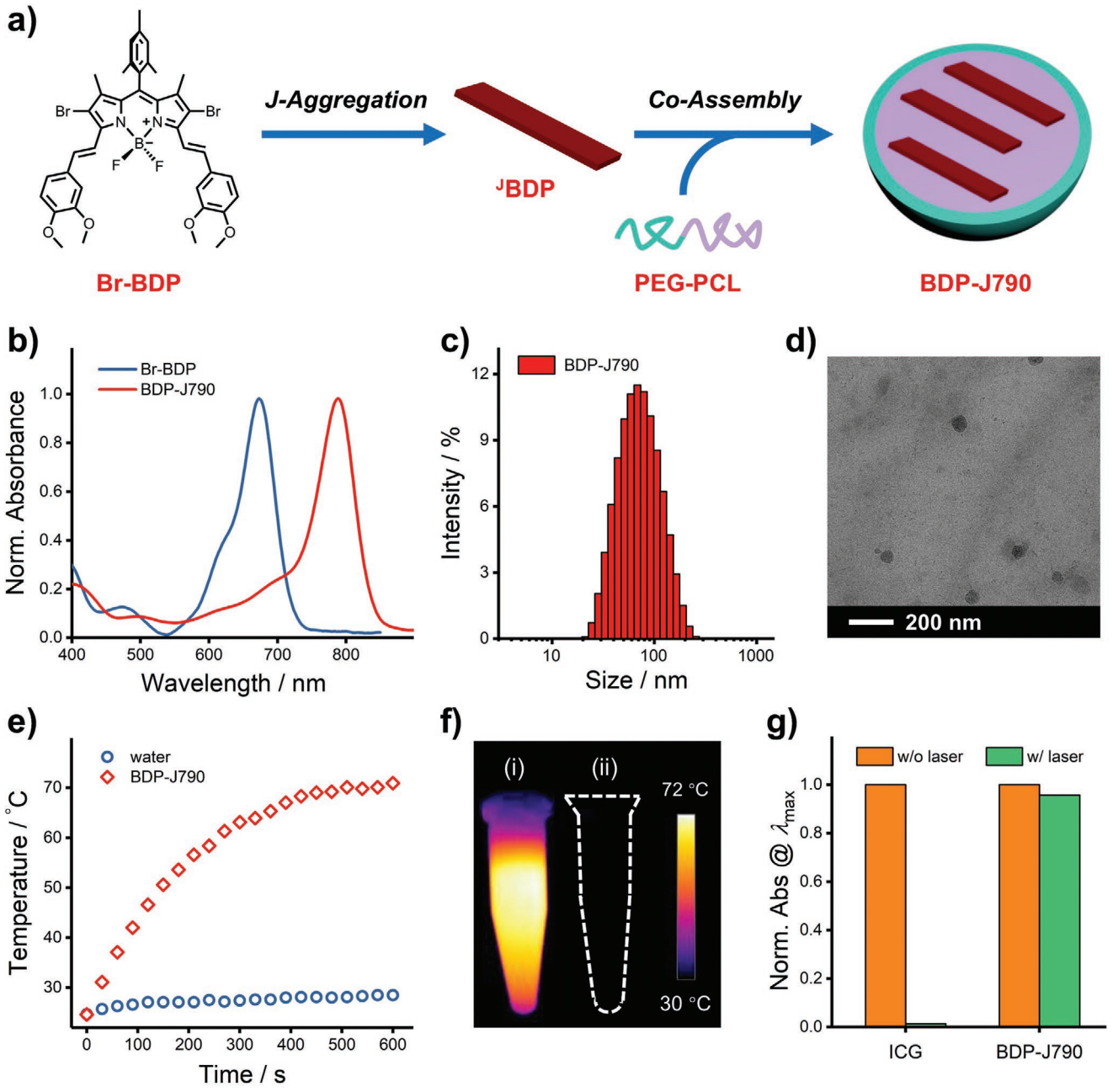

Figure 2. a) Schematic illustration of the preparation of a water-stable polymeric nanoparticle (BDP-J790) with Br-BDP J-aggregates embedded in the hydrophobic core. b) Normalized UV–vis absorption spectra of Br-BDP in DMF and BDP-J790 in water. c) Size distribution and d) representative TEM image of BDP-J790 nanoparticle. e) Temperature elevations recorded for BDP-J790 (3.5 μM Br-BDP) upon laser-2 irradiation. f) IR thermal images of i) BDP-J790 and ii) water after 10 min laser-2 irradiation in the same conditions as (e). g) Relative absorbance changes recorded for aqueous solutions of BDP-J790 (3.5 μM Br-BDP) and ICG (with a same absorbance at 785 nm) after 30 min laser-2 irradiation. Laser-2: 785 nm, 1.8 W cm^{-2}.

living system.[51–55] In our previous work, we reported that the J-aggregation of BODIPY dyes yielded a pure organic PTA with striking performance including red-shifted absorbance into the NIR region, high PCE, and significant resistance against photobleaching.[56–58] We thus employed BODIPY J-aggregates as the photothermal component of the nanosystem (**Figure 2**a). Possessing two bromine atoms at the 2,6-positions, the Br-BDP can readily form slip-stacked J-aggregate through π–π stacking and halogen-bonding interactions,[58,59] as evidenced by the drastic 117 nm redshift of the absorption maximum (Figure 2b). An amphiphilic PEG-PCL was then used to stabilize the Br-BDP J-aggregate to obtain a water-stable nanoparticle (BDP-J790) with controlled size of 80 nm (Figure 2c,d; see Supporting Information).

We then evaluated the photothermal performance of BDP-J790 by using an IR thermal camera to record the solution temperature. Upon IR thermal imaging, the photo-induced temperature elevation of BDP-J790 dispersion (3.5 μM Br-BDP)

after laser-2 irradiation (785 nm; 1.8 W cm^{-2}; 10 min) can be visualized (Figure 2f). The quantitative temperature elevation versus irradiation time was also recorded, and it demonstrated that the solution temperature can rise to 70.9 °C at 10 min (Figure 2e), which is high enough to trigger the thermolysis of EPO-3 (Figure S7d, Supporting Information). By contrast, the temperature of pure water upon laser irradiation in the same condition was elevated only to 28.5 °C (Figure 2e). The PCE of BDP-J790 was calculated to be ≈59.8% (Figure S8, Supporting Information),[60] which is relatively high among reported organic PTAs.[61–66] In addition to photothermal efficiency, photothermal stability is another concern in our design to ensure constant photo-release of trapped $^1O_2$. We collected the UV–vis absorption spectra (Figure 2g and Figure S9b, Supporting Information) and size distribution (Figure S9a, Supporting Information) of BDP-J790 before and after 30 min laser-2 irradiation. Gratifyingly, negligible changes were observed for the BDP-J790, in stark contrast to FDA approved ICG dye, which suffered severe photobleaching (Figure 2g and Figure S9c, Supporting Information). Collectively, the above results have demonstrated the efficient photothermal property of BDP-J790 containing J-aggregated BODIPY dyes.

2.3. Construction of the Target Photosensitive Polymeric Carrier

Encouraged by the above findings, we moved to prepare the desired photosensitive polymeric carrier with a sustained $^1O_2$-production regulated by two NIR beams for enhanced antitumor phototherapy. To achieving such a sophisticated function, three key components, that is, a PS (I-BDP) to generate $^1O_2$, a reservoir to store $^1O_2$, and a PTA to release the stored $^1O_2$, should be orchestrated in one single nanosystem. As depicted in **Figure 3**a, based on the strategy of co-assembly with an amphiphilic PEG-PCL, the desired polymeric nanoparticle (An-NP) embedded with a PS (I-BDP), a reservoir (An-3), and a PTA (J-aggregated Br-BDP; denoted as ^{J}BDP) within the hydrophobic core was successfully obtained. Transmission electron microscopy (TEM) revealed a nanoparticle morphology of 120 nm in diameter (Figure 3b), and DLS measurement gave an intensity-average hydrodynamic diameter of 140 nm (Figure 3c). It is worth of noting that the size of 140 nm should benefit the antitumor application of An-NP in vivo as it meets the criteria for the EPR (enhanced permeability and retention) effect, which endows nanoparticle with the ability to passively target tumor issue.[67] Moreover, the UV–vis absorption spectrum of An-NP showed the characteristic absorption bands of An-3, I-BDP, and ^{J}BDP (Figure 3d), indicating the encapsulation of the three key components and the stability of the J-aggregation of Br-BDP. The loading content and encapsulation efficiency of the three components in An-NP have been estimated (Table S1, Supporting Information). In addition, inappreciable changes in the size of An-NP in PBS, cell-culture medium, or fetal bovine serum were observed (Figure 3e and Figure S10, Supporting Information), suggesting its significant colloidal stability.

We further assessed the photodynamic and photothermal performance of the final An-NP, which were controlled by two NIR beams (laser-1 and laser-2), respectively. A water soluble $^1O_2$ indicator (QDPBF)[57] was adopted to evaluate the photosensitivity. Considering that the spectral overlap between QDPBF and An-3 of An-NP may affect the $^1O_2$ determination, we then prepared I-BDP micelle (see the Supporting Information) as the An-NP mimic to evaluate the photosensitivity of I-BDP. As shown in Figure 3f and Figure S11, Supporting Information, QDPBF was significantly consumed upon laser-1 irradiation (3 mW cm^{-2}), indicating the efficient photoactivity of An-NP in generation of $^1O_2$ due to the I-BDP component. After laser-2 irradiation (1.8 W cm^{-2}), An-NP displayed excellent photothermal conversion ability (PCE = 59.3%) due to the ^{J}BDP component (Figure 3g,h; Figures S12 and S13, Supporting Information). Moreover, upon 5 cycling of photo-mediated heating and cooling, negligible changes in the photothermal performance (Figure S14a, Supporting Information), nanoparticle size (Figure S14c, Supporting Information), and absorption spectra (Figure S14b, Supporting Information) were found, indicating that the multiple photothermal processes did not affect the structure and performance of the An-NP material.

2.4. Remotely Controlled $^1O_2$ Trapping/Releasing Through Two NIR Beams In Vitro

Having established the efficient photogeneration of $^1O_2$ during laser-1-inducted photosensitizing process of the I-BDP component of An-NP and significant heat generation during laser-2-triggered photothermal process of the ^{J}BDP component, we then investigated the two NIR beams-controlled $^1O_2$ trapping/releasing performance given by the An-3 component (**Figure 4**a). Upon laser-1 irradiation, An-3 component trapped the I-BDP-generated abundant $^1O_2$ to form EPO-3 as demonstrated by the time-dependent attenuation of the absorption of An-3 (Figure 4b). Subsequently, upon laser-2 irradiation, the heat generated by the ^{J}BDP component triggered the thermolysis of EPO-3 of EPO-NP, releasing the stored $^1O_2$ and recovering An-3 (Figure 4c), which will work in the next $^1O_2$ storing/releasing cycle. After demonstrating the renewability of the An-3 component and the photo-mediated reversible $^1O_2$ trapping/releasing properties of An-NP in solution (Figure 4d and Figure S15, Supporting Information), we continued to apply it in living cells.

HeLa cells were incubated with An-NP for 4 h, and the efficient cellular uptake of An-NP was demonstrated by the fluorescence of An-3 in cells through confocal imaging (Figure S16, Supporting Information). DCF-DA was used as a fluorescence indicator of $^1O_2$ to estimate the photo-controlled release of $^1O_2$ in living cells.[57,68,69] HeLa cells were divided into three groups for different treatments as outlined in **Figure 5**a (also see Supporting Information). In group 1, the cells were incubated with An-NP and DCF-DA, then exposed to laser-1 irradiation (10 mW cm^{-2}) for 5 min. Intense green fluorescence of the oxidized DCF was observed (Figure 5b i), indicating the effective $^1O_2$ generation during the laser-1-induced PDT process. On the contrary, HeLa cells pretreated with sodium azide (NaN_3; $^1O_2$ scavenger[70]) displayed undetectable fluorescence upon laser-1 irradiation, further verifying the photosensitized $^1O_2$ generation of An-NP (Figure 5c and Figure S17, Supporting Information). In group 2, the cells were incubated with EPO-NP (for its preparation, see the Supporting Information) and DCF-DA, then subjected to laser-2 irradiation (1.0 W cm^{-2}) or incubated in dark for 10 min before

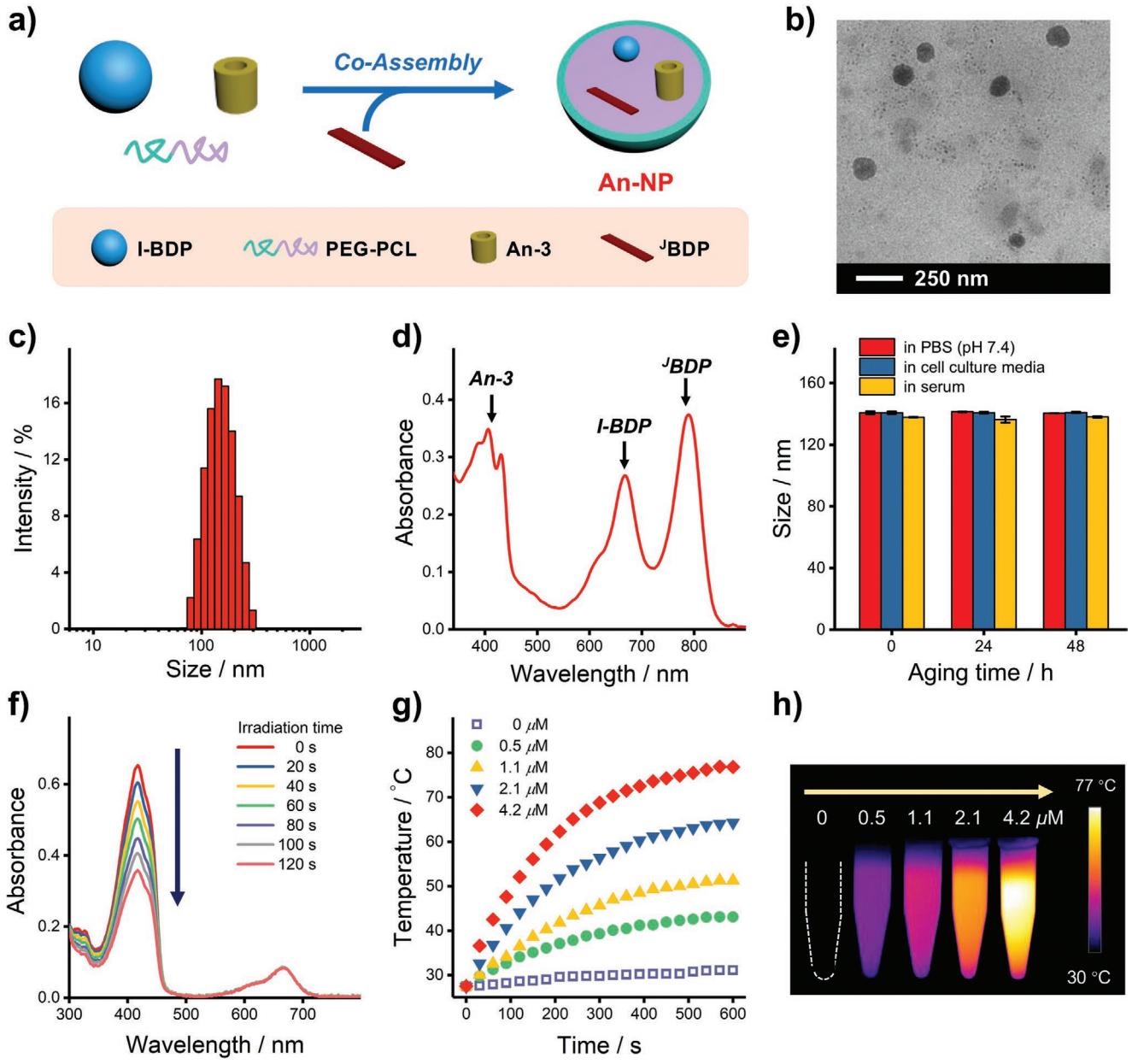

Figure 3. a) Schematic illustration of the preparation of the target water-stable photosensitive polymeric nanoparticle (An-NP) with An-3, I-BDP, and Br-BDP J-aggregates embedded in the hydrophobic core. b) Typical TEM image, c) size distribution, and d) UV–vis absorption spectra of An-NP. e) Time-evolution of the particle size of An-NP in PBS, cell culture media, or fetal bovine serum. Error bars represent mean ± SD ($n = 3$). f) Time-dependent UV–vis absorption spectra of QDPBF within the aqueous solution of I-BDP micelle upon laser-1 irradiation. g) Temperature elevations recorded for BDP-J790 at different concentrations of Br-BDP upon laser-2 irradiation. h) IR thermal images of BDP-J790 at different concentrations of Br-BDP after 10 min laser irradiation in the same conditions as (e). Laser-1: 655 nm, 3 mW cm^{-2}; laser-2: 785 nm, 1.8 W cm^{-2}.

imaging. Compared with undetectable fluorescence in the cells without laser treatment (Figure 5d and Figure S18, Supporting Information), the DCF fluorescence within the cells after laser-2 irradiation was strong (Figure 5b ii). Moreover, pretreatment with sodium azide could substantially reduce the DCF fluorescence (Figure 5d and Figure S18, Supporting Information). The above results clearly indicated that laser-2 irradiation could efficiently induce the $^1O_2$ release from EPO-NP in living cells owing to the photoconverted heat which triggered the cycloreversion of EPO-3 embedded in EPO-NP.

In group 3, the cells were incubated with An-NP and exposed to laser-1 irradiation (10 mW cm^{-2}) for 10 min, then stained with DCF-DA, followed by laser-2 irradiation (1.0 W cm^{-2}) for 10 min. No detectable DCF fluorescence was observed before laser-2 irradiation (Figure 5e and Figure S19, Supporting Information), and a clear DCF fluorescence was observed after laser-2 irradiation (Figure 5b iii and Figure S19, Supporting Information). The above findings demonstrated that in living cells, the internalized An-NP can be converted into EPO-NP by capturing $^1O_2$ during laser-1-induced PDT process, which can

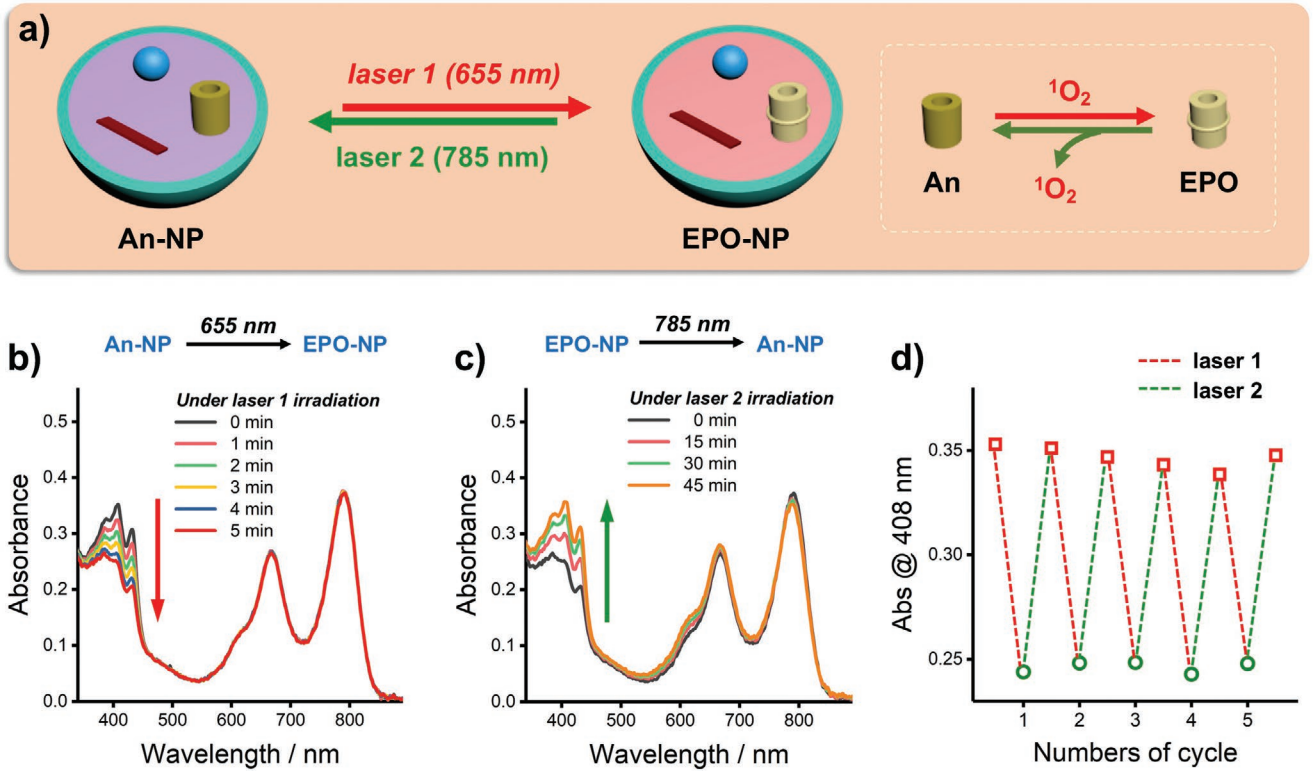

Figure 4. a) Schematic illustration of the interconversion between An-NP and EPO-NP regulated by two NIR laser beams. b) Evaluation of the laser-1-triggered An-NP-to-EPO-NP transition and c) laser-2-induced EPO-NP-to-An-NP conversion by UV–vis spectroscopy. d) Absorbance changes of An-3 embedded in An-NP upon repeated cycles of laser-1 irradiation for 5 min and laser-2 irradiation for 35 min. Laser-1: 655 nm, 10 mW cm^{-2}; laser-2: 785 nm, 1.8 W cm^{-2}.

readily release the trapped $^1O_2$ in the laser-2-driven PTT process. Moreover, we prepared a control nanoparticle (-An)-NP without An-3 being encapsulated (see the Supporting Information), and compared its PDT-induced intracellular $^1O_2$ generation ability and in vitro photocytotoxicity with An-NP. As expected, both (-An)-NP and An-NP micelles produced abundant $^1O_2$ in living cells upon laser-1 irradiation, and no detectable changes in the photogenerated $^1O_2$ amount (Figure S20, Supporting Information) and photocytotoxicity (Figure S21, Supporting Information) were observed, indicating that An-3 did not affect the in vitro treatment outcome ascribed to the generated $^1O_2$ during PDT process. Notably, all HeLa cells in different experimental groups without nanoparticles or laser treatment showed inappreciable fluorescence of DCF (Figure 5c–e and Figures S17–S19, Supporting Information), suggesting that the nanoparticles and laser beams did not interfere with the $^1O_2$ detection. The sustained $^1O_2$ generation capability of An-NP enables the $^1O_2$ stored in PDT process to be constantly released in the interval between two PDT processes which is used for the oxygen replenishment.

In addition to controlling the release of $^1O_2$ from EPO-NP in the interval of PDT processes, laser-2 can induce the PTT effect of An-NP and/or EPO-NP, might further enhance the overall outcome of the anticancer phototherapy. We then investigated the laser-2-mediated in vitro photocytotoxicity resulted from the released $^1O_2$ and PTT, respectively, by MTT assay. HeLa cells were incubated with An-NP or EPO-NP for 4 h, then exposed to laser-2 irradiation (1.0 W cm^{-2}) for 10 min. As shown in **Figure 6**, PTT effect of the ^{J}BDP component within An-NP resulted in 40.5% inhibition of cell viability. While for EPO-NP, laser-2 irradiation in the same condition caused 69.4% inhibition of cell viability (Figure 6). Considering that An-3 to EPO-3 conversion within the nanoparticle did not affect the J-aggregation of Br-BDP which contribute the photothermal effect (Figure 4b), we speculated that the cytotoxicity induced by the PTT effect of EPO-NP should be close to that induced by the PTT effect of An-NP. Thereby, compared with the photocytotoxicity of An-NP, the extra 28.9% viability inhibition caused by EPO-NP should be attributed to the 785 nm laser-released $^1O_2$. Pretreatment of $^1O_2$ scavenger, that is, NaN_3, effectively reduced the cytotoxicity of EPO-NP upon laser-2 irradiation, with the inhibition of cell viability decreased to 44.6% (Figure 6). This finding further demonstrated the efficient $^1O_2$ release from EPO-NP during laser-2 irradiation, which induced distinct cytotoxicity to cancer cells.

2.5. In Vivo Antitumor Phototherapy

We further studied the antitumor phototherapeutic efficacy of An-NP in vivo. First, low-dose An-NP (3.0 mg/kg ^{J}BDP) was injected intravenously into 4T1 tumor-bearing Balb/c mice to assess the tumor accumulation of the nanoagent by recording the PTT-induced temperature elevations. IR thermal images

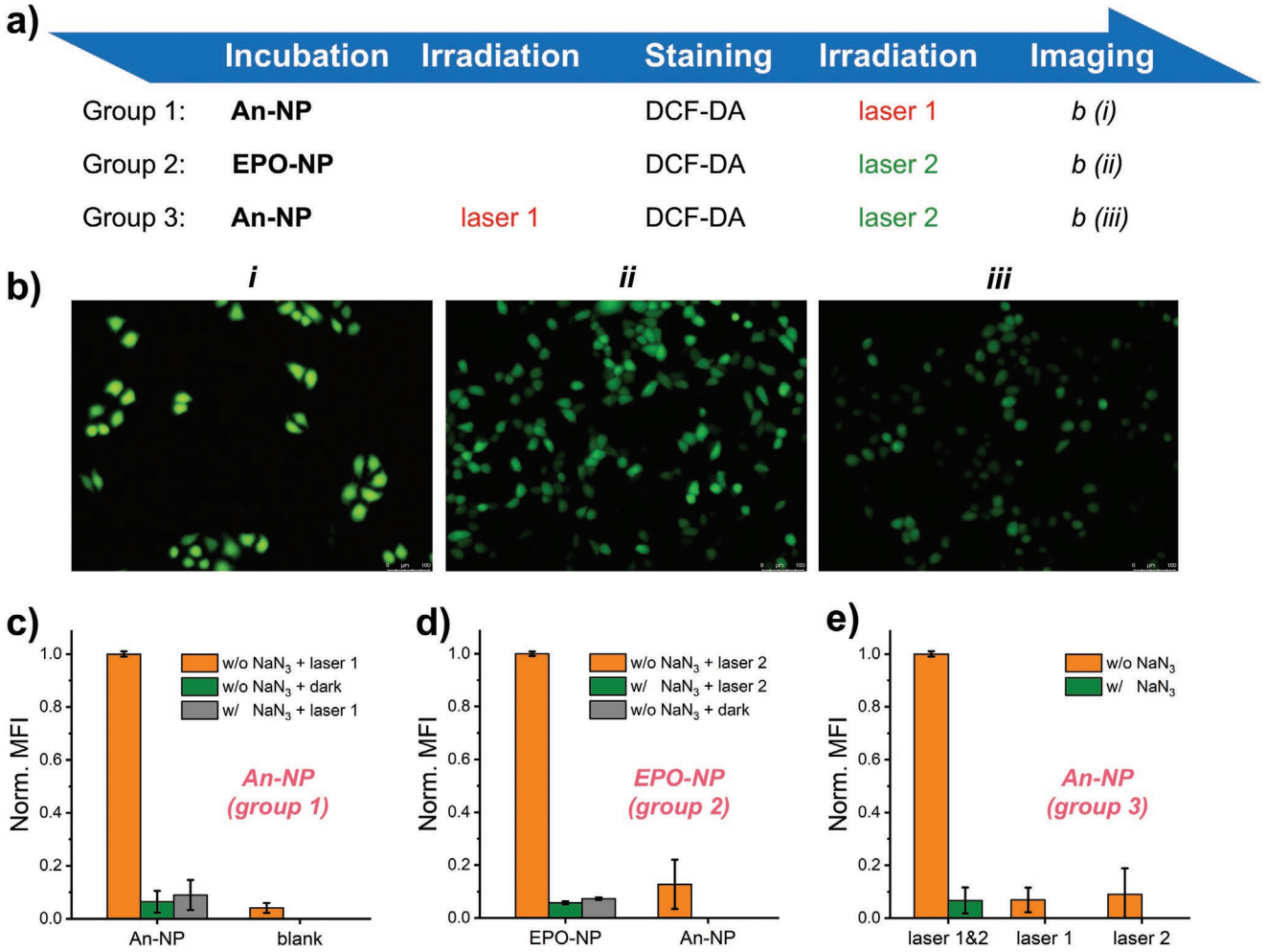

Figure 5. a) Summary and b) typical fluorescence images of the DCF-DA staining experiments to determine the intracellular $^1O_2$ produced via the photosensitizing process of An-NP (group 1) or via the photo-releasing process of EPO-NP (groups 2 and 3). Group 1: laser-1 irradiation for 5 min; Group 2: laser-2 irradiation for 10 min; Group 3: pre-irradiated by laser-1 for 10 min and laser-2 irradiation for 10 min. c–e) Normalized mean fluorescence intensity (Norm. MFI) calculated from DCF-DA staining fluorescence images of HeLa cells after different treatments as indicated. Laser-1: 655 nm, 10 mW cm^{-2}; laser-2: 785 nm, 1.0 W cm^{-2}.

were recorded after irradiation of laser–2 (0.5 W cm^{-2}; 5 min) at different time points post intravenous injection, and the time-dependent thermal images of the mice were shown in Figure S23a, Supporting Information. After administration of An-NP, obvious PTT-induced temperature elevations were found at the tumor site and reached a maximum post 8 h of injection (Figure S23b, Supporting Information). The observation indicated that An-NP was stable during the blood circulation, and could be accumulated at the tumor site owing to EPR effect.[67] For mice treated with higher dose of An-NP (6.0 mg/kg ^{J}BDP) for 8 h, the mean temperature at the tumor sites rose from 38.1 to 50.7 °C (**Figure 7**a,b), allowing thermolysis of EPO to release $^1O_2$.

The antitumor phototherapy of An-NP controlled by two NIR laser beams was further investigated. After the xenograft 4T1 tumor grew to ≈100 mm^3, the mice were randomly divided into four groups for different treatments: i) treated with PBS (200 µL) only, ii) treated with PBS and lasers irradiation (laser-1 for 10 min, followed by laser-2 for 10 min), iii) treated with An-NP (200 µL, 6.0 mg/kg) only, and iv) treated with An-NP and lasers irradiation (laser-1 for 10 min, followed by laser-2 for 10 min). After 8 h of the intravenous injection of PBS or An-NP (6.0 mg/kg ^{J}BDP), the tumors were exposed to laser-1 irradiation (10 mW cm^{-2}; 10 min) and subsequent laser-2 irradiation (0.5 W cm^{-2}; 10 min). The changes in the tumor volume were recorded to evaluate the phototherapy efficacies. For group iv), the tumors regressed and eliminated 2 and 4 days after the laser treatment, respectively (Figure 7c,d and Figure S24, Supporting Information), and no tumor recurrence was observed. On the contrary, similar to PBS-treatment, treatment solely with An-NP or laser irradiation did not inhibit the tumor growth as reflected by the observation of continuous tumor growth (Figure 7c). After two weeks of observation, all the mice in different groups were sacrificed and the xenograft tumors were collected if still have (Figure 7d and Figure S25, Supporting Information), showing that the tumors completely disappeared in group (iv). Taken together, the above results demonstrated an efficient antitumor phototherapy of An-NP nanoagent controlled by two NIR beams.

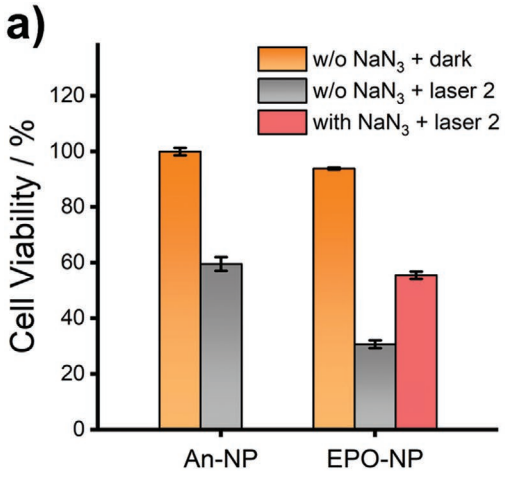

b)

	w/o NaN_3 dark	w/o NaN_3 laser 2	w/ NaN_3 laser 2
An-NP	/	***PTT***	/
	0%	40.5%	/
EPO-NP	/	***PTT + $^1O_2$***	***PTT***
	6.1%	69.4%	44.6%

Figure 6. a) Cell viability of An-NP- or EPO-NP-treated HeLa cells after different treatments as indicated ($n = 4$). b) Summary of the treatment modalities as well as the cell-inhibition efficiencies, which were calculated by the formula: (1 – cell viability) × 100%.

Notably, during two weeks of observation, no appreciable loss in body weight was found for all mice in different groups (Figure S26, Supporting Information), indicating that An-NP is biocompatible. Moreover, to further evaluate the biosafety of An-NP, the main organs (heart, liver, spleen, lung, and kidney) of the sacrificed mice were collected for histological hematoxylin and eosin (H&E) analysis (Figure 7e). As expected, no obvious pathological changes were observed from all H&E sections. The above results confirmed the biocompatibility of An-NP nanoagent

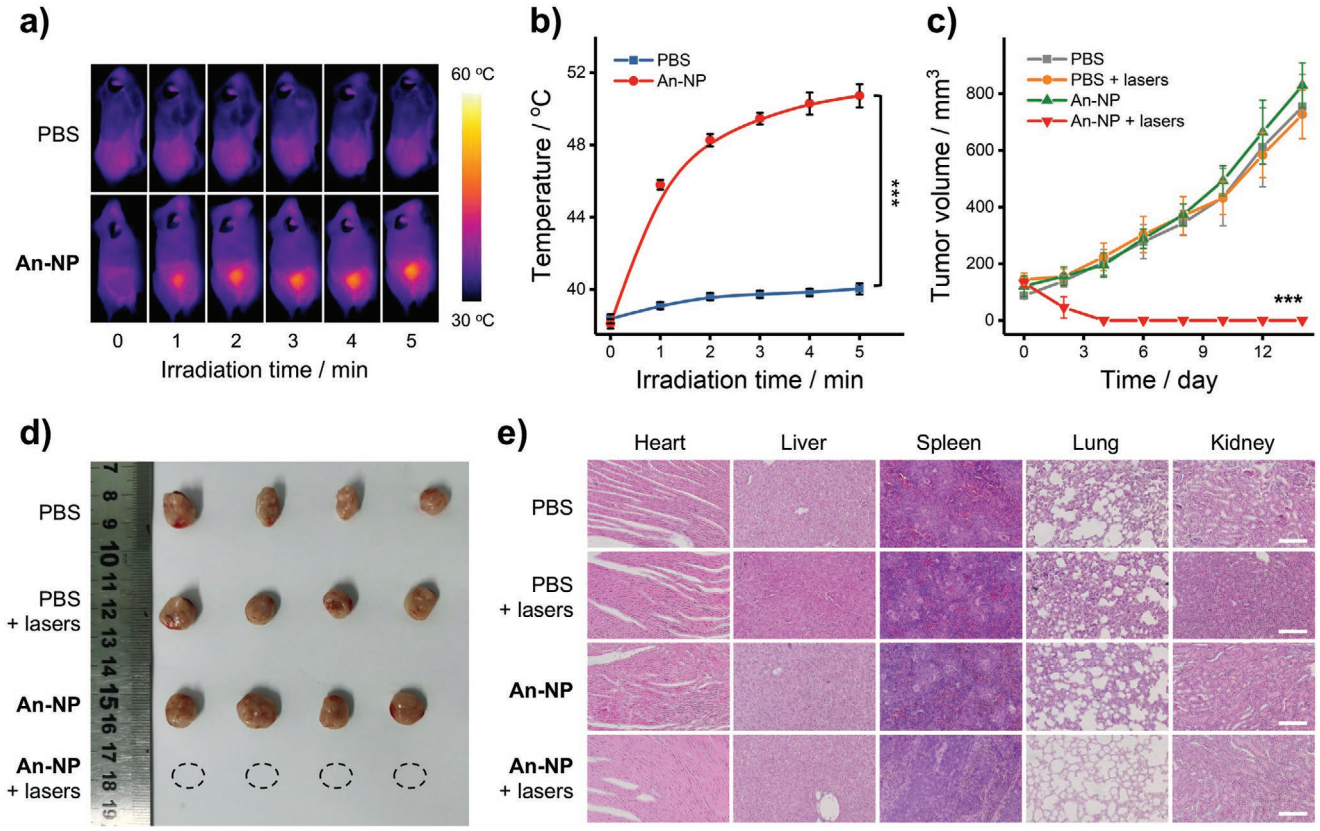

Figure 7. a) Typical IR thermal images and b) mean temperatures of the tumor regions recorded for xenograft tumor-bearing mice treated without or with An-NP (6.0 mg/kg ^{1}BDP) under laser-2 irradiation. c) Time-dependent changes in the tumor volume of mice in different groups. d) Optical photographs of stark tumors collected after 2-week observation. e) H&E costaining images of major organs. Scale bar: 200 µm. Data represents mean ± SD ($n = 4$), ***$P < 0.001$ (one-way ANOVA). Laser-2: 785 nm, 0.5 W cm^{-2}.

in antitumor phototherapy. As controls, the antitumor performances of single PDT of An-NP, single PTT of An-NP, and combinational PDT/PTT of (-An)-NP were studied. As shown in Figure S27, Supporting Information, single PDT of An-NP, single PTT of An-NP, and combinational PDT/PTT of (-An)-NP inhibited tumor growth. However, none of them achieved tumor elimination as synergistic phototherapy of (An)-NP did, demonstrating the unique synergistic antitumor phototherapy efficacy of An-NP.

3. Conclusions

In this work, we have successfully prepared a novel photosensitive polymeric carrier with a sustained $^1O_2$-production regulated by two NIR beams for enhanced antitumor phototherapy. By co-assembling with an amphiphilic diblock copolymer, three key components, that is, a PS (I-BDP) to generate $^1O_2$, a reservoir (An-3) to store $^1O_2$, and a PTA (^{l}BDP) to release the stored $^1O_2$, were orchestrated in a single nanosystem to yield the sophisticated nanomaterial (An-NP). We demonstrated that in both solution and living cells, upon 655 nm laser irradiation, the PDT process of An-NP occurred to generate abundant $^1O_2$ with extra $^1O_2$ being stored via the formation of EPO-NP; while in the subsequent 785 nm laser-driven PTT process, the converted EPO-NP underwent thermolysis to release the trapped $^1O_2$ and recover An-NP. The oxygen level can be replenished in the PTT process for the next round of PDT to generate $^1O_2$. The presented photosensitive nanomaterial allows alternative application of PDT and PTT controlled by two NIR laser beams, thus enabling sufficient oxygen supply and sustained $^1O_2$ generation during the entire synergistic phototherapy. The nanomaterial was further applied to antitumor phototherapy in vivo and demonstrated striking efficacy.

Supporting Information

Supporting Information is available from the Wiley Online Library or from the author.

Acknowledgements

Financial support from National Natural Science Foundation of China (Grant 51673101) and the Fundamental Research Funds for Central Universities (Nankai University, Grant 92022030) is gratefully acknowledged. All animal experiments were carried out in compliance with the guide for the care and use of laboratory animals of Tianjin Science and Technology Commission.

Conflict of Interest

The authors declare no conflict of interest.

Data Availability Statement

The data that support the findings of this study are available from the corresponding author upon reasonable request.

Keywords

photoactive, photodynamic therapy, photothermal therapy, polymeric nanoparticles, singlet oxygen

Received: February 26, 2021
Revised: April 15, 2021
Published online: June 18, 2021

[1] X. S. Li, S. Y. Lee, J. Yoon, *Chem. Soc. Rev.* **2018**, *47*, 1174.
[2] A. P. Castano, P. Mroz, M. R. Hamblin, *Nat. Rev. Cancer* **2006**, *6*, 535.
[3] T. F. Zhang, Y. Y. Li, Z. Zheng, R. Q. Ye, Y. R. Zhang, R. T. K. Kwok, J. W. Y. Lam, B. Z. Tang, *J. Am. Chem. Soc.* **2019**, *141*, 5612.
[4] D. van Straten, V. Mashayekhi, H. S. de Bruijn, S. Oliveira, D. J. Robinson, *Cancers* **2017**, *9*, 19.
[5] Á. Juarranz, P. Jaén, F. Sanz-Rodríguez, J. Cuevas, S. González, *Clin. Transl. Oncol.* **2008**, *10*, 148.
[6] Y. S. Dong, Y. L. Tu, K. W. Wang, C. F. Xu, Y. Y. Yuan, J. Wang, *Angew. Chem., Int. Ed.* **2020**, *59*, 7168.
[7] Y. Cai, D. Q. Ni, W. Y. Cheng, C. D. Ji, Y. L. Wang, K. Müllen, Z. Q. Su, Y. Liu, C. Y. Chen, M. Z. Yin, *Angew. Chem., Int. Ed.* **2020**, *59*, 14014.
[8] Y. Yang, W. J. Zhu, L. Cheng, R. Cai, X. Yi, J. X. He, X. S. Pan, L. Yang, K. Yang, Z. Liu, W. H. Tan, M. W. Chen, *Biomaterials* **2020**, *246*, 119971.
[9] P. Agostinis, K. Berg, K. A. Cengel, T. H. Foster, A. W. Girotti, S. O. Gollnick, S. M. Hahn, M. R. Hamblin, A. Juzeniene, D. Kessel, M. Korbelik, J. Moan, P. Mroz, D. Nowis, J. Piette, B. C. Wilson, J. Golab, *Ca-Cancer J. Clin.* **2011**, *61*, 250.
[10] D. Hanahan, R. A. Weinberg, *Cell* **2000**, *100*, 57.
[11] H. Harada, M. Inoue, S. Itasaka, K. Hirota, A. Morinibu, K. Shinomiya, L. H. Zeng, G. F. Ou, Y. X. Zhu, M. Yoshimura, W. G. McKenna, R. J. Muschel, M. Hiraoka, *Nat. Commun.* **2012**, *3*, 783.
[12] K. Kiyose, K. Hanaoka, D. Oushiki, T. Nakamura, M. Kajimura, M. Suematsu, H. Nishimatsu, T. Yamane, T. Terai, Y. Hirata, T. Nagano, *J. Am. Chem. Soc.* **2010**, *132*, 15846.
[13] J. Pouysségur, F. Dayan, N. M. Mazure, *Nature* **2006**, *441*, 437.
[14] S. S. Wang, H. Liu, J. Mack, J. W. Tian, B. Zou, H. Lu, Z. F. Li, J. X. Jiang, Z. Shen, *Chem. Commun.* **2015**, *51*, 13389.
[15] J. Xu, S. B. Sun, Q. Li, Y. Yue, Y. D. Li, S. J. Shao, *Analyst* **2015**, *140*, 574.
[16] G. Q. Zhang, G. M. Palmer, M. W. Dewhirst, C. L. Fraser, *Nat. Mater.* **2009**, *8*, 747.
[17] X. C. Zheng, X. Wang, H. Mao, W. Wu, B. R. Liu, X. Q. Jiang, *Nat. Commun.* **2015**, *6*, 5834.
[18] K. Y. Zhang, P. L. Gao, G. L. Sun, T. W. Zhang, X. L. Li, S. J. Liu, Q. Zhao, K. K.-W. Lo, W. Huang, *J. Am. Chem. Soc.* **2018**, *140*, 7827.
[19] P. Vaupel, O. Thews, M. Hoeckel, *Med. Oncol.* **2001**, *18*, 243.
[20] Z. J. Zhou, J. B. Song, L. M. Nie, X. Y. Chen, *Chem. Soc. Rev.* **2016**, *45*, 6597.
[21] H. He, S. S. Ji, Y. He, A. J. Zhu, Y. L. Zou, Y. B. Deng, H. T. Ke, H. Yang, Y. L. Zhao, Z. Q. Guo, H. B. Chen, *Adv. Mater.* **2017**, *29*, 1606690.
[22] X. Z. Zhao, S. R. Long, M. L. Li, J. F. Cao, Y. C. Li, L. Y. Guo, W. Sun, J. J. Du, J. L. Fan, X. J. Peng, *J. Am. Chem. Soc.* **2020**, *142*, 1510.
[23] R. Sullivan, C. H. Graham, *Cancer Metastasis Rev.* **2007**, *26*, 319.
[24] A. L. R. de Souza, K. Marra, J. Gunn, K. S. Samkoe, S. C. Kanick, S. C. Davis, M. S. Chapman, E. V. Maytin, T. Hasan, B. W. Pogue, *Br. J. Cancer* **2016**, *115*, 805.
[25] Z. W. Xiao, S. Halls, D. Dickey, J. Tulip, R. B. Moore, *Clin. Cancer Res.* **2007**, *13*, 7496.

[26] L. Y. Yang, Y. C. Wei, D. Xing, Q. Chen, *Lasers Surg. Med.* **2010**, *42*, 671.
[27] C. Li, X. C. Zheng, W. Z. Chen, S. L. Ji, Y. Yuan, X. Q. Jiang, *Nano Lett.* **2020**, *20*, 6526.
[28] I. S. Turan, D. Yildiz, A. Turksoy, G. Gunaydin, E. U. Akkaya, *Angew. Chem., Int. Ed.* **2016**, *55*, 2875.
[29] Z. Yuan, S. Yu, F. Y. Cao, Z. W. Mao, C. Y. Gao, J. Ling, *Polym. Chem.* **2018**, *9*, 2124.
[30] S. Martins, J. P. S. Farinha, C. Baleizao, M. N. Berberan-Santos, *Chem. Commun.* **2014**, *50*, 3317.
[31] L. Slavetinska, J. Mosinger, P. Kubat, *J. Photochem. Photobiol., A* **2008**, *195*, 1.
[32] J. M. Aubry, C. Pierlot, J. Rigaudy, R. Schmidt, *Acc. Chem. Res.* **2003**, *36*, 668.
[33] W. Fudickar, T. Linker, *Chem. - Eur. J.* **2011**, *17*, 13661.
[34] D. Zehm, W. Fudickar, M. Hans, U. Schilde, A. Kelling, T. Linker, *Chem. - Eur. J.* **2008**, *14*, 11429.
[35] L. Slavetinska, J. Mosinger, M. Dracinsky, M. Posta, *J. Inclusion Phenom. Macrocyclic Chem.* **2008**, *61*, 241.
[36] W. Fudickar, T. Linker, *J. Org. Chem.* **2017**, *82*, 9258.
[37] W. Fudickar, T. Linker, *J. Am. Chem. Soc.* **2012**, *134*, 15071.
[38] S. Kolemen, T. Ozdemir, D. Lee, G. M. Kim, T. Karatas, J. Yoon, E. U. Akkaya, *Angew. Chem., Int. Ed.* **2016**, *55*, 3606.
[39] A. M. Asadirad, Z. Erno, N. R. Branda, *Chem. Commun.* **2013**, *49*, 5639.
[40] Y. Li, X. M. Liu, L. Tan, Z. D. Cui, X. J. Yang, Y. F. Zheng, K. W. K. Yeung, P. K. Chu, S. L. Wu, *Adv. Funct. Mater.* **2018**, *28*, 1800299.
[41] V. Arkhipova, H. Fu, M. W. H. Hoorens, G. Trinco, L. N. Lameijer, E. Marin, B. L. Feringa, G. J. Poelarends, W. Szymanski, D. J. Slotboom, A. Guskov, *J. Am. Chem. Soc.* **2021**, *143*, 1513.
[42] P. Y. Lam, A. R. Thawani, E. Balderas, A. J. P. White, D. Chaudhuri, M. J. Fuchter, R. T. Peterson, *J. Am. Chem. Soc.* **2020**, *142*, 17457.
[43] K. Aggarwal, T. P. Kuka, M. Banik, B. P. Medellin, C. Q. Ngo, D. Xie, Y. Fernandes, T. L. Dangerfield, E. Ye, B. Bouley, K. A. Johnson, Y. J. Zhang, J. K. Eberhart, E. L. Que, *J. Am. Chem. Soc.* **2020**, *142*, 14522.
[44] J. Morstein, M. A. Dacheux, D. D. Norman, A. Shemet, P. C. Donthamsetti, M. Citir, J. A. Frank, C. Schultz, E. Y. Isacoff, A. L. Parrill, G. J. Tigyi, D. Trauner, *J. Am. Chem. Soc.* **2020**, *142*, 10612.
[45] R. C. Sarott, A. E. G. Viray, P. Pfaff, A. Sadybekov, G. Rajic, V. Katritch, E. M. Carreira, J. A. Frank, *J. Am. Chem. Soc.* **2021**, *143*, 736.
[46] K. R. Deng, Z. Y. Hou, X. R. Deng, P. P. Yang, C. X. Li, J. Lin, *Adv. Funct. Mater.* **2015**, *25*, 7280.
[47] K. Hayashi, M. Nakamura, H. Miki, S. Ozaki, M. Abe, T. Matsumoto, T. Kori, K. Ishimura, *Adv. Funct. Mater.* **2014**, *24*, 503.
[48] Z. He, L. L. Zhao, Q. Zhang, M. J. Chang, C. X. Li, H. S. Zhang, Y. Lu, Y. S. Chen, *Adv. Funct. Mater.* **2020**, *30*, 1910301.
[49] Y. X. Xu, X. L. Liang, P. Bhattarai, Y. Sun, Y. M. Zhou, S. M. Wang, W. Chen, H. Y. Ge, J. R. Wang, L. G. Cui, Z. F. Dai, *Adv. Funct. Mater.* **2017**, *27*, 1704096.
[50] C. Y. Yang, Y. D. Chen, W. Guo, Y. Gao, C. Q. Song, Q. Zhang, N. N. Zheng, X. J. Han, C. S. Guo, *Adv. Funct. Mater.* **2018**, *28*, 1706827.
[51] S. C. Zhang, Q. Z. Li, N. Yang, Y. H. Shi, W. Ge, W. J. Wang, W. Huang, X. J. Song, X. C. Dong, *Adv. Funct. Mater.* **2019**, *29*, 1906805.
[52] Y. J. Liu, P. Bhattarai, Z. F. Dai, X. Y. Chen, *Chem. Soc. Rev.* **2019**, *48*, 2053.
[53] X. T. Gao, S. S. Jiang, C. Y. Li, Y. z. Chen, Y. F. Zhang, P. Huang, J. Lin, *Biomaterials* **2021**, *267*, 120454.
[54] L. Y. Zhao, Y. M. Liu, R. Chang, R. R. Xing, X. H. Yan, *Adv. Funct. Mater.* **2019**, *29*, 1806877.
[55] H. S. Jung, P. Verwilst, A. Sharma, J. Shin, J. L. Sessler, J. S. Kim, *Chem. Soc. Rev.* **2018**, *47*, 2280.
[56] X. S. Yan, M. H. Su, Y. N. Liu, Y. K. Zhang, H. Zhang, C. H. Li, *Adv. Funct. Mater.* **2021**, *31*, 2008406.
[57] M. H. Su, S. X. Li, H. Zhang, J. Q. Zhang, H. L. Chen, C. H. Li, *J. Am. Chem. Soc.* **2019**, *141*, 402.
[58] M. H. Su, Q. J. Han, X. S. Yan, Y. N. Liu, P. Luo, W. H. Zhai, Q. Z. Zhang, L. Y. Li, C. H. Li, *ACS Nano* **2021**, *15*, 5032.
[59] M. H. Su, X. S. Yan, X. Guo, Q. W. Li, Y. S. Zhang, C. H. Li, *Chem. - Eur. J.* **2020**, *26*, 4505.
[60] Y. Lyu, C. Xie, S. A. Chechetka, E. Miyako, K. Pu, *J. Am. Chem. Soc.* **2016**, *138*, 9049.
[61] Y. Jiang, P. K. Upputuri, C. Xie, Z. L. Zeng, A. Sharma, X. Zhen, J. C. Li, J. G. Huang, M. Pramanik, K. Y. Pu, *Adv. Mater.* **2019**, *31*, 1808166.
[62] X. X. Yao, P. Yang, Z. K. Jin, Q. Jiang, R. R. Guo, R. H. Xie, Q. J. He, W. L. Yang, *Biomaterials* **2019**, *197*, 268.
[63] S. Y. Ye, J. M. Rao, S. H. Qiu, J. L. Zhao, H. He, Z. L. Yan, T. Yang, Y. B. Deng, H. T. Ke, H. Yang, Y. L. Zhao, Z. Q. Guo, H. B. Chen, *Adv. Mater.* **2018**, *30*, 1801216.
[64] Q. L. Zou, M. Abbas, L. Y. Zhao, S. K. Li, G. Z. Shen, X. H. Yan, *J. Am. Chem. Soc.* **2017**, *139*, 1921.
[65] X. Cai, A. Bandla, C. K. Chuan, G. Magarajah, L.-D. Liao, D. B. L. Teh, B. K. Kennedy, N. V. Thakor, B. Liu, *Mater. Horiz.* **2019**, *6*, 311.
[66] Z. B. Zha, X. L. Yue, Q. S. Ren, Z. F. Dai, *Adv. Mater.* **2013**, *25*, 777.
[67] J. Fang, H. Nakamura, H. Maeda, *Adv. Drug Delivery Rev.* **2011**, *63*, 136.
[68] Y. H. Cheng, H. Cheng, C. X. Jiang, X. F. Qiu, K. K. Wang, W. Huan, A. H. Yuan, J. H. Wu, Y. Q. Hu, *Nat. Commun.* **2015**, *6*, 8785.
[69] N. M. Idris, M. K. Gnanasammandhan, J. Zhang, P. C. Ho, R. Mahendran, Y. Zhang, *Nat. Med.* **2012**, *18*, 1580.
[70] W. H. Zhai, Y. K. Zhang, M. Liu, H. Zhang, J. Q. Zhang, C. H. Li, *Angew. Chem., Int. Ed.* **2019**, *58*, 16601.